J|A|C|S
ARTICLES

Published on Web 05/12/2009

Structure-Based Rationale for Selectivity in the Asymmetric Allylic Alkylation of Cycloalkenyl Esters Employing the Trost 'Standard Ligand' (TSL): Isolation, Analysis and Alkylation of the Monomeric form of the Cationic η^3-Cyclohexenyl Complex $[(\eta^3\text{-}c\text{-}C_6H_9)Pd(TSL)]^+$

Craig P. Butts,[†] Emane Filali,[†] Guy C. Lloyd-Jones,*[,†] Per-Ola Norrby,*[,‡] David A. Sale,[†] and York Schramm[†]

School of Chemistry, University of Bristol, Cantock's Close, Bristol, BS8 1TS, U.K., and Department of Chemistry, University of Gothenburg, Kemigården 4, SE-412 96 Göteborg, Sweden

Received December 29, 2008; E-mail: guy.lloyd-jones@bris.ac.uk; pon@chem.gu.se

Abstract: The solution-phase structures of the monomeric forms of the cationic Pd-η^3-allyl and Pd-η^3-cyclohexenyl complexes [Pd(*R,R*)-**1**(η^3-C_3H_5)]$^+$ (**7**$^+$) and [Pd(*R,R*)-**1**(η^3-C_6H_9)]$^+$ (**8**$^+$) bearing the *trans*-cyclohexylenediamine-based Trost 'Standard Ligand' (*R,R*)-**1** have been elucidated by NMR, isotopic labeling and computation. In both complexes, (*R,R*)-**1** is found to adopt a C_1-symmetric conformation, leading to a concave shape in the 13-membered chelate in which one amide group in the chiral scaffold projects its NH unit out of the concave surface in close vicinity to one allyl terminus. The adjacent amide has a reversed orientation and projects its carbonyl group out of the concave face in the vicinity of the opposite allyl terminus. Stoichiometric and catalytic asymmetric alkylations of [**8**$^+$][X$^-$] by $MCHE_2$ (E = ester, M = 'escort' counterion, X = Pd allyl counterion) show the same selectivities and trends as have been reported for in situ-generated catalysts, and a new model for the enantioselectivity has been explored computationally. Three factors are found to govern the regioselectivity (*pro-S* vs *pro-R*) of attack of nucleophiles on the η^3-C_6H_9 ring in **8**$^+$ and thus the *ee* of the alkylation product: (i) a *pro-R* torquoselective bias is induced by steric interaction of the η^3-C_6H_9 moiety with one phenyl ring of the ligand; (ii) *pro-S* delivery of the nucleophile can be facilitated by hydrogen-bonding with the concave orientated amide N−H; and (iii) *pro-R* delivery of the nucleophile can be facilitated by escort ion (M) binding to the concave orientated amide carbonyl. The latter two opposing interactions lead to the selectivity of the alkylation being sensitive to the identities of X$^-$ and M$^+$. The generation of **8**$^+$ from cyclohexenyl ester substrate has also been explored computationally. The concave orientated amide N−H is able to activate the leaving group of the allylic ester by hydrogen bonding to its carbonyl group. However, this interaction is only feasible for the (*S*)-enantiomer of substrate, leading to the prediction of a powerful kinetic resolution ($k_S \gg k_R$), as is found experimentally. This new model involving two regiochemically distinct (NH) and (CO) locations for nucleofuge or nucleophile binding, may prove of broad utility for the interpretation of the selectivity in asymmetric allylic alkylation reactions catalyzed by Pd complexes of (*R,R*)-**1** and related ligands.

1. Introduction

Since its inception in 1992, the Trost Modular Ligand series ("TML", Chart 1)[1] has been applied to an extraordinary range of asymmetric allylic alkylation reactions[2] and is among the small group of chiral ligands that offer genuine utility for asymmetric transition-metal catalyzed C−C bond-formation.[3] It has been especially successful with allylic substrates that have proven difficult to control with other systems,[2] and the *trans*-diaminocyclohexane-based 'Standard Ligand' (**1**) has, in most cases, been found to provide very high selectivities, under carefully optimized conditions.[4]

The generally accepted mechanism for Pd-catalyzed allylic alkylation can be abbreviated[5] to a cycle involving two key steps: oxidative addition of a low valent Pd species, "$L_2Pd(0)$", to the allylic electrophile and nucleophilic attack on the resulting Pd(II) allyl cation, to liberate the product and regenerate the Pd(0) complex. For reactions involving allylic esters (typically carboxylates and carbonates) and stabilized nucleophiles (typically stabilized enolates, such as malonates), the overall stereochemical pathway is one of retention, arising from 2-fold inversion.[6] Within this framework, there are opportunities for asymmetric induction at both stages of the reaction.[2,4] Thus, for the oxidative addition event, asymmetric catalysis can

[†] University of Bristol.
[‡] University of Gothenburg.

(1) Trost, B. M.; Van Vranken, D. L. *Angew. Chem. Int Ed.* **1992**, *31*, 228.
(2) Recent reviews. (a) Lu, Z.; Ma, S. *Angew Chem., Int. Ed.* **2008**, *47*, 258. (b) Trost, B. M.; Lee, C. *Catalytic Asymmetric Synthesis*, 2nd ed; Ojima; I., Ed.; Wiley-VCH: New York, 2000; pp 593−649. (c) Pfaltz; A.; Lautens, M. *Comprehensive Asymmetric Catalysis*; Jacobsen, E. N., Pfaltz, A., Yamamoto, H., Eds.; Springer: Heidelberg, 1999; pp 833−886.

Chart 1. Trost Modular Ligand Series ('TML') and 'Standard Ligand' **1**, with 'Wall' and 'Flap' Rings Indicated

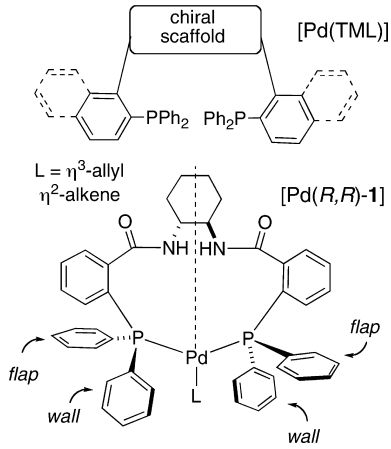

Scheme 1. Trost and Bunt's Asymmetric Allylic Alkylation of Racemic Cycloalkenyl Esters (X = Acetate or Methyl Carbonate) Using Catalytic Pd(*R,R*-**1**) to Induce Highly *pro-S* Selective Attack on 'Meso'-**2** by Malonate or Phthalimide Nucleophiles (Nu)[9]

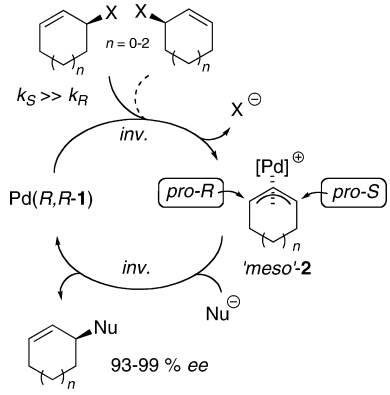

proceed by for example enantioface selection in prochiral substrates, kinetic resolution, or desymmetrization. In the nucleophilic attack on the Pd-allyl species, selectivity can be induced for example by allyl enantioface selection, allyl regioselection (*pro-R* vs *pro-S*), or nucleophile enantioface selection. What distinguishes the TML series from the vast range of other ligands developed for asymmetric allylic alkylation[2] is that it has proven utility[3,4] in all of these regimes, including use of O- and N-based nucleophiles[4] as well as 'harder' nucleophiles such as enolates[7] and lithiated methylpyridines.[8] As a consequence, it has enjoyed widespread application in synthesis.[3,4]

A major development in the field came in 1994, when Trost and Bunt[9] demonstrated that unprecedented levels of enantioselectivity (93−99% ee) could be achieved in the reaction of

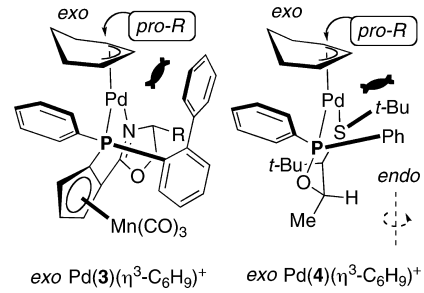

Figure 1. Pd(η^3-*c*-C_6H_9) complexes of the P,X-ligands **3**[12] and **4**[13] designed for asymmetric alkylation of cycloalkenyl esters, illustrating the two control elements: exo/endo biasing and activation trans to P.

simple cycloalkenyl esters with malonate and phthalimide nucleophiles, Scheme 1. Such reactions in principle[10] proceed via a single Pd-η^3-cycloalkenyl cationic intermediate (**2**), thus while kinetic resolution of cycloalkenyl ester may attend the process,[11] the enantio-determining step is the nucleophilic attack on the 'meso' Pd-η^3-cycloalkenyl moiety (**2**) to generate the alkylation product. The product enantiomer ratio is thus determined by the regioselectivity of attack at the *pro-R* versus *pro-S* allylic terminus, the formal meso symmetry[10a] of the Pd-η^3-cycloalkenyl moiety (**2**) being broken by the chirality of the appended ligand (**1**).

It later emerged that other ligands could also exert a high degree of stereocontrol in these previously troublesome reactions involving 'slim' cyclic allylic substrates.[2] However, in contrast to P,P-based ligand **1**, the use of a mixed donor 'P,X' ligand system (where P is a phosphorus-based donor and X is a heteratom such as N or S) was required to achieve high enantioselectivities (>95% ee). Prime examples are the cymantrene-based phosphinoaryl oxazolines (**3**) developed by Helmchen,[12] and the phosphinite sulfides (**4**), developed by Evans,[13] illustrated for alkylation of Pd(η^3-*c*-C_6H_9) in Figure 1.

In both cases (**3**[12] and **4**[13]), through the systematic study of structure-selectivity relationships, single crystal X-ray analysis and NMR spectroscopy of intermediates, two synergistic effects were confirmed as essential components in the overall performance and design of the ligand. First, steric interactions between the ligand and the cycloalkenyl moiety must strongly disfavor one rotameric isomer (endo) over the other (exo) in the [(P,X)Pd(η^3-cycloalkenyl)]$^+$ intermediate. Second, with the η^3-cycloalkenyl unit orientated in the exo isomer with respect to the ligand framework, and thus the *pro-R* vs *pro-S* allylic termini orientated in the square plane with respect to the P and X donors, one allylic terminus is more activated than the other to nucleophilic attack, due to its trans relationship with the P. This combination of η^3-cycloalkenyl orientation with terminus-specific activation can then induce the

(3) At the time of submission (Dec 2008), Chemical Abstracts listed over 205 publications reporting on the efficient application of "Pd(**1**)" in asymmetric catalysis.
(4) For leading references, see: Trost, B. M.; Crawley, M. L. *Chem. Rev.* **2003**, *103*, 2921.
(5) Evans, L. A.; Fey, N.; Harvey, J. N.; Hose, D.; Lloyd-Jones, G. C.; Murray, P.; Orpen, A G.; Osborn, R.; Owen-Smith, G. J. J.; Purdie, M. *J. Am. Chem. Soc.* **2008**, *130*, 14471, and references therein.
(6) (a) Trost, B. M.; Weber, L.; Strege, P. E.; Fullerton, T. J.; Dietsche, T. J. *J. Am. Chem. Soc.* **1978**, *100*, 3416. (b) Mackenzie, P. B.; Whelan, J.; Bosnich, B. *J. Am. Chem. Soc.* **1985**, *107*, 2046. (c) Hayashi, T.; Yamamoto, A.; Hagihara, T. *J. Org. Chem.* **1986**, *51*, 723.
(7) Trost, B. M.; Schroeder, G. M. *Chem.−Eur. J.* **2005**, *11*, 174.
(8) Trost, B. M.; Thaisrivongs, D. A. *J. Am. Chem. Soc.* **2008**, *130*, 14092.
(9) Trost, B. M.; Bunt, R. C. *J. Am. Chem. Soc.* **1994**, *116*, 4089.
(10) (a) Trost, B. M.; Bunt, R. C. *J. Am. Chem. Soc.* **1996**, *118*, 235. (b) Lloyd-Jones, G. C.; Stephen, S. C. *Chem.−Eur. J.* **1998**, *4*, 2539. (c) Fristrup, P.; Jensen, T.; Hoppe, J.; Norrby, P.-O. *Chem.−Eur. J.* **2006**, *12*, 5352, and references therein.
(11) (a) Dominguez, B.; Hodnett, N. S.; Lloyd-Jones, G. C. *Angew. Chem., Int. Ed.* **2001**, *40*, 4289. (b) Lloyd-Jones, G. C.; Stephen, S. C. *Chem. Commun.* **1998**, 2321. (c) Gais, H.-J.; Eichelmann, H.; Spalthoff, N.; Gerhards, F.; Frank, M.; Raabe, G. *Tetrahedron: Asymmetry* **1998**, *9*, 235. (d) Frank, M.; Gais, H.-J. *Tetrahedron: Asymmetry* **1998**, *9*, 3353. (e) Gais, H. J.; Spalthoff, N.; Jagusch, T.; Frank, M.; Raabe, G. *Tetrahedron Lett.* **2000**, *41*, 3809.
(12) Kudis, S.; Helmchen, G. *Angew. Chem., Int. Ed.* **1998**, *37*, 3047.
(13) Evans, D. A.; Campos, K. R.; Tedrow, J. S.; Michael, F. E.; Gagne, M. R. *J. Am. Chem. Soc.* **2000**, *122*, 7905.

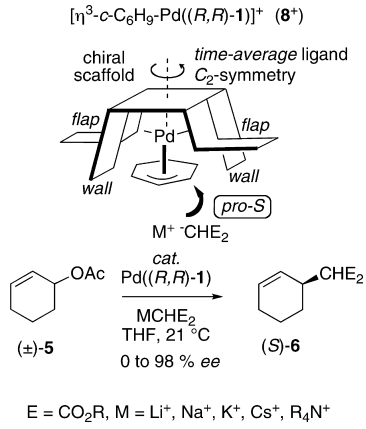

Figure 2. Wall-and-flap cartoon model[20] for asymmetric alkylation involving Pd complexes of (*R,R*)-**1**, with the asymmetric alkylation of cyclohexenyl acetate (**5**) as an example.

requisite regioselectivity, to generate the alkylation product in high ee.[12,13] In light of this analysis, it is tempting to ascribe an analogous mode of selectivity by ligand **1**, whereby it acts as a P,O-bidentate ligand, via coordination of one of the amide carbonyl groups. However, results from the systematic removal of various ligand components,[10b,14] the isolation of a catalytically active but nonenantioselective binuclear bis-*P,O*-Pd-allyl complex of **1**,[15] and preliminary ^{31}P NMR spectroscopic studies,[16] strongly support the active and selective species to be P,P-, not P,O-coordinated Pd complexes.

In contrast to the detailed structural and spectroscopic data obtained in the study of the mechanism of selectivity of most of the other classes of ligand for asymmetric Pd-catalyzed allylation, the analysis of the asymmetric induction by **1**, in all of its numerous successful applications,[3,4] has been made extremely challenging due to a paucity of pertinent structural data.[16,17] Thus, despite extensive but largely unrewarding efforts to structurally characterize the intermediates involved in catalysis by Pd(**1**),[10b,15−18] rationalization has, by necessity, been achieved by way of empirical correlation. In 1999 Trost and Toste[17] replaced a first-generation mnemonic that simply predicted torquoselectivity on the basis of ligand configuration,[19] with a second-generation three-dimensional model based coordination of **1** to generate a chiral pocket around the η^2-alkene/η^3-allyl coordination plane.[17,20] The time-averaged structure of coordinated ligand **1** is represented by a C_2-symmetric folded surface,[20] Figure 2, in which selectivity is based on a steric deactivation mechanism. The four phenyl rings play key roles by adopting pseudoaxial ('wall') and pseudoequatorial ('flap') orientations (see Chart 1), with the 'walls' acting to selectively impede egress

Chart 2. Cationic Monomeric Palladium η^3-Allyl (**7**) and η^3-Cyclohexenyl (**8**) Complexes of the Standard Ligand (*R,R*)-**1** Generated in situ from Oligomer, then Studied by NMR

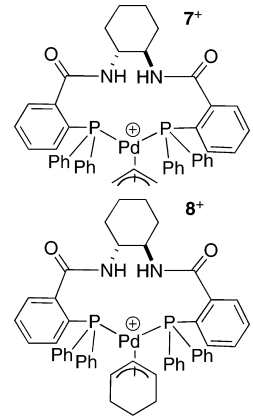

of nucleofuge and entry of nucleophile in one front and one rear quadrant of the allyl plane.

This 'cartoon model'[17] has broad application in that it can be used to rationalize the outcome from nearly all of the optimized reactions catalyzed by Pd(**1**) and related ligands in the TML series.[20] As an example, the reaction of *rac*-cyclohexenyl acetate (±)-(**5**) with malonate nucleophile ($MCHE_2$, E = CO_2Me or CO_2Bn, M = 'escort' cation), is correctly predicted to proceed with powerful kinetic resolution of **5** ($k_{S/R} \geq 45$ with *R,R*-**1**),[11] and selective nucleophilic attack by $MCHE_2$ at the *pro-S* terminus (→(*S*)-**6**).[9]

Despite the undeniable utility of the cartoon model,[20] detailed information about the intermediates involved in the reactions would allow a structural basis for rationalization of the selectivity, and facilitate further development and application of the ligand class. However, the complexity of the system, vide infra, demands that such a study begins with a simple example comprising solely the basic components necessary for the reaction. The reaction of cyclohexenyl acetate (**5**) with $MCHE_2$ to generate (*S*)-**6** (Figure 2) fulfils this requirement.[9] Moreover, it also provides the challenge that any new model must a priori predict that the *pro-S* selectivity is M^+-dependent,[9] a fact not easily rationalized by the current cartoon model,[20] with the ee of (*S*)-**6** rising from 0−98% ee in the order: $Li^+ < Na^+ < K^+ < Cs^+ < R_4N^+$ (R = *n*-Bu, *n*-Hex.).

Herein we report on a combined computational and $^2H/^{13}C$ label-facilitated NMR analysis of Pd((*R,R*)-**1**) complexes bearing η^3-allyl and η^3-cyclohexenyl moieties (**7**$^+$ and **8**$^+$, Chart 2).The structural details are then allied with computational and experimental analyses of the generation of the η^3-cyclohexenyl complex **8**$^+$ from *rac*-cyclohexenyl acetate (±)-(**5**), and the *pro-S* selective addition of $MCHE_2$, to develop a model for the catalytic process (±)-**5**→(*S*)-**6**, Figure 2. We also show that the model may be of utility in the rationalization and prediction of the much broader range of asymmetric allylic alkylation reactions catalyzed by Pd(*R,R*)-**1**.[3,4]

2. Results and Discussion

To date, structural details for the key intermediates in the asymmetric alkylation reaction mediated by Pd(**1**), namely the η^3-allylic complexes, have remained elusive.[10,16,17,21] Indeed, ^1H NMR spectra of even apparently simple Pd allyl complexes of **1** are reported as uninterpretable[17] due to, inter alia, overlap with signals from numerous other species.[16] We earlier reported

(14) Trost, B. M.; Breit, B.; Organ, M. G. *Tetrahedron Lett.* **1994**, *35*, 5817.
(15) Butts, C. P.; Crosby, J.; Lloyd-Jones, G. C.; Stephen, S. C. *Chem. Commun.* **1999**, 1707.
(16) (a) Fairlamb, I. J. S.; Lloyd-Jones, G. C. *Chem. Commun.* **2000**, 2447. (b) Lloyd-Jones, G. C.; Stephen, S. C.; Fairlamb, I. J. S.; Martorell, A.; Dominguez, B.; Tomlin, P. M.; Murray, M.; Fernandez, J. M.; Jeffery, J. C.; Riis-Johannessen, T.; Guerziz, T. *Pure. Appl. Chem.* **2004**, *76*, 589.
(17) Trost, B. M.; Toste, F. D. *J. Am. Chem. Soc.* **1999**, *121,* 4545 and footnotes 15 and 18 and associated text therein.
(18) Amatore, C.; Jutand, A.; Mensah, L.; Ricard, L. *J. Organomet. Chem.* **2007**, *692*, 1457.
(19) Trost, B. M. *Acc. Chem. Res.* **1996**, *29*, 355.
(20) Trost, B. M.; Machacek, M. R.; Aponick, A. *Acc. Chem. Res.* **2006**, *39*, 747.

Chart 3. Enantiomerically Pure, d_5-Phenyl Bearing Isotopologues of Ligand (*R*,*R*)-**1**, Prepared for NMR Studies of $\mathbf{7}^+$ and $\mathbf{8}^+$

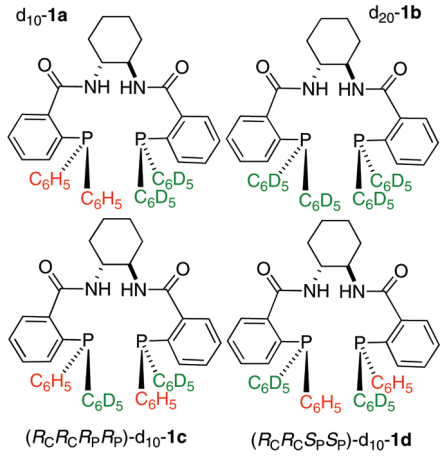

that the effect of temperature and concentration on both the net optical rotatory power and the $^{31}P\{^1H\}$ NMR spectra of solutions of η^3-allyl complexes ($\mathbf{7}^+$) clearly indicates that the system has a high propensity for reversible aggregation or oligomerization;[16,22] the η^3-cyclohexenyl complex ($\mathbf{8}^+$), the key intermediate involved in the conversion of cyclohexenyl acetate (**5**) to (*S*)-**6**, Figure 2, behaves analogously. We also proposed that catalytic turnover via these oligomeric complexes can substantially reduce the selectivity in asymmetric allylic alkylation reactions involving Pd(**1**), thus accounting for the inverse dependence of selectivity and catalyst loading that has been observed in such reactions.[16] The goal of the study reported herein was to study the structure and reactivity of the *monomeric* Pd allyl complexes of **1**, and three issues had therefore to be addressed: first, the complexes must be generated free from signal overlap by oligomeric and aggregated complexes, second, it needed to be confirmed that the species studied were indeed the monomeric complexes ($\mathbf{7}^+$) and ($\mathbf{8}^+$), and third a number of deuterated forms of ligand (*R*,*R*)-**1** were required to facilitate the detailed NMR analysis of complexes $\mathbf{7}^+$ and $\mathbf{8}^+$, vide infra.

Synthesis of ^{2}H-Labeled Ligand (*R*,*R*)-1. In addition to a perdeuterated η^3-cyclohexenyl system, vide infra, four enantiomerically pure deuterated forms of **1** were prepared—d_{10}-**1a**, d_{20}-**1b**, d_{10}-**1c**, and d_{10}-**1d**, Chart 3. The synthesis of each required preparation of the appropriate d_5- or d_{10}-*ortho*-diphenylphosphino benzoic acid (**9**) to combine with known procedures for amide coupling with (*R*,*R*)-cyclohexane diamine.[23] By adaptation of the procedure of Rauchfuss for the synthesis of unlabeled **9** from PPh_3,[24] the perdeuterodiphenyl derivative d_{10}-**9** was readily prepared from d_{15}-PPh_3 and then coupled with the requisite amines[23,25] to generate isotopically desymmetrized ligand d_{10}-**1a** and the symmetrical ligand d_{20}-**1b**.

Scheme 2. Synthesis of *P*-Chiral d_5-*ortho*-Diphenylphosphino Benzoic Acids (R_P)-d_5-**9** and (S_P)-d_5-**9**[a]

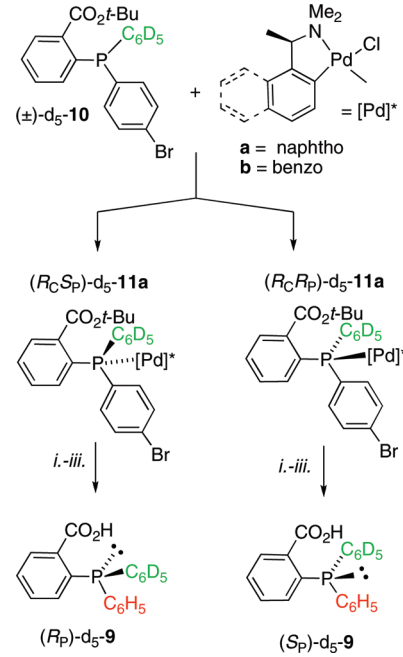

[a] Conditions: (i) 100 equiv of $H_2NCH_2CH_2NH_2$;[30] (ii) 8 equiv of KOH in THF;[31] (iii) BuLi, THF, −78 °C, AcOH.

The preparation of the benzoic acids (R_P)-d_5-**9** and (S_P)-d_5-**9**, *P*-chiral through isotopic substitution, proved significantly more challenging. All attempts to adapt known methods for the asymmetric synthesis of *P*-chiral phosphines using stereospecific displacements of chiral auxiliaries[26] failed. We thus developed a procedure involving resolution, Scheme 2. Key to the strategy was the use of a *p*-Br substituent on the nondeuterated phenyl ring as a 'traceless resolving handle', so as to overcome the inherent low-grade chirality arising solely from isotopic substitution. Using a *tert*-butyl ester to protect the carboxylic acid, we assembled (±)-d_5-**10** from $(Et_2N)_2PCl$, via a repeated sequence of substituting of Cl with Ar, using ArMgX reagents, then Et_2N with Cl, using anhydrous HCl in ether.[27] With (±)-d_5-**10** in hand, resolution was achieved by employing the method of Ibers and Otsuka,[28] for which the 1-naphthyl analogue **11a**[29] proved efficient for diastereomer separation via column chromatography.

Both diastereomers of **11a** were microcrystalline or amorphous, so *P*-configurations were assigned by X-ray diffraction studies on a single crystal of the much more crystalline benzo complex **11b**·Et_2O. This same crystal (ca. 3 μg) was then dissolved in CD_2Cl_2 and analyzed by $^{31}P\{^1H\}$ NMR to allow assignment of the ^{31}P chemical shifts of (R_C,R_P)-**11b**/(R_C,S_P)-**11b**. After decomplexation of the separated diastereomers of **11a**, the absolute configurations of the resulting (R_P)-d_5-**10** and (S_P)-d_5-**10** were assigned by $^{31}P\{^1H\}$ NMR by recomplexation

(21) Molecular mechanics structures of several allyl complexes of Pd-**1** and analogues have been calculated: Helena Hagelin, "Palladium-Catalyzed Aromatic Coupling and Allylic Substitution—An Experimental and Theoretical Study" Ph D. thesis, Royal Inst. of Technology, Stockholm, Sweden, 1999.
(22) A detailed analysis of the anion, solvent, temperature and concentration-dependencies of the monomer−oligomer populations will be reported in due course.
(23) Trost, B. M.; Van Vranken, D. L.; Bingel, C. *J. Am. Chem. Soc.* **1992**, *114*, 9327.
(24) Hoots, J. E.; Rauchfuss, T. B.; Wrobleski, T. B. *Inorg. Syntheses* **1982**, *21*, 175.
(25) Correia, J. D. G.; Domingos, A.; Santos, I. *Eur. J. Inorg. Chem.* **2000**, 1523.
(26) For a recent review, see. (a) Johansson, M. J.; Kann, N. C. *Mini-Reviews In Organic Chemistry* **2004**, *1*, 233.
(27) Markl, G.; Amrhein, J.; Stoiber, T.; Striebl, U.; Kreitmeier, P. *Tetrahedron* **2002**, *58*, 2551.
(28) Tani, K.; Brown, L. D.; Ahmed, J.; Ibers, J. A.; Yokota, M.; Nakamura, A.; Otsuka, S. *J. Am. Chem. Soc.* **1977**, *99*, 7876.
(29) Alcock, N. W.; Brown, J. M.; Hulmes, D. I. *Tetrahedron Asym.* **1993**, *4*, 743.
(30) Dunina, V. V.; Kuz'mina, L. G.; Rubina, M. Y.; Grishin, Y. K.; Veits, Y. A.; Kazakova, E. I. *Tetrahedron Asym.* **1999**, *10*, 1483.
(31) Filali, E.; Lloyd-Jones, G. C.; Sale, D. A. *Synlett* **2009**, 205.

Scheme 3. Synthesis of Oligomeric Cationic Pd(**1**)-Allyl BAr′F Complexes

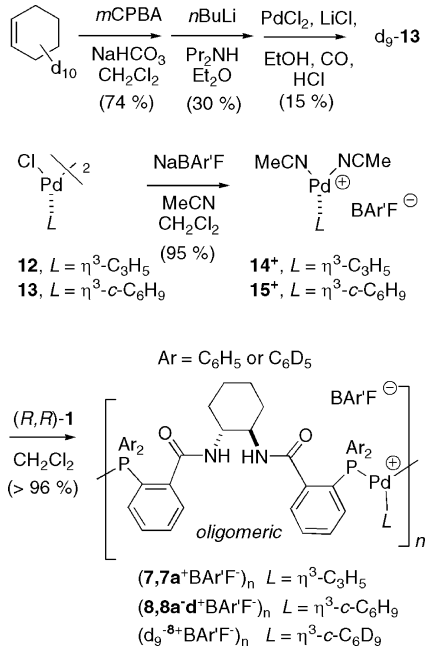

to generate **11b**. Finally, *tert*-butyl ester hydrolysis[31] then protodebromination gave samples of (R_P)-d_5-**9** and (S_P)-d_5-**9** (≥95% ee) which were coupled with (*R*,*R*)-cyclohexanediamine[23] to give ($R_CR_CR_PR_P$)-d_{10}-**1c** and ($R_CR_CS_PS_P$)-d_{10}-**1d** in high diastereoisotopomeric purity.

Preparation of Pd-Allyl Complexes 7$^+$ and 8$^+$. In earlier work we found that coordinating counterions increase the equilibrium population of higher-order species in the simple allyl complex **7**$^+$. Key to our present investigation has been the very low interactivity of the [B((3,5-(CF$_3$)$_2$)C$_6$H$_3$)$_4$]$^-$ anion ("BAr′F")[32] with Pd-allyl cations,[5] which has allowed us to prepare monomeric complexes, relatively free of oligomer.[16] As shown in Scheme 3, reaction of the readily prepared allylic palladium chloride complexes [(η^3-C$_3$H$_5$)PdCl]$_2$ (**12**)[33] and [(η^3-*c*-C$_6$H$_9$)-PdCl]$_2$ (**13**)[33] with NaBAr′F affords the cationic complexes [(η^3-C$_3$H$_5$)Pd(MeCN)$_2$][BAr′F] (**14**$^+$[BAr′F$^-$]) and [(η^3-*c*-C$_6$H$_9$)Pd-(MeCN)$_2$][BAr′F] (**15**$^+$[BAr′F$^-$]) as white amorphous solids.These stable precursors react cleanly with ligand (*R*,*R*)-**1** in CH_2Cl_2 to afford the oligomeric complexes (**7**$^+$BAr′F$^-$)$_n$ and (**8**$^+$BAr′F$^-$)$_n$ as glassy solids, in high yield (>96%). By preparation of d_9-cyclohex-2-enol from d_{10}-cyclohexene, we also generated, via d_9-**13** and d_9-**15**, the perdeuterated η^3-cyclohexenyl isomer (d_9-**8**$^+$BAr′F$^-$)$_n$, and using ligands d_{10}-**1a**, d_{20}-**1b**, d_{10}-**1c**, and d_{10}-**1d** (Chart 3) the isotopologous complexes (d_{10}-**7a**)$_n$, (d_{10}-**8a**$^+$BAr′F$^-$)$_n$, (d_{20}-**8b**$^+$BAr′F$^-$)$_n$, (d_{10}-**8c**$^+$BAr′F$^-$)$_n$, and (d_{10}-**8d**$^+$BAr′F$^-$)$_n$.

Oligomeric complexes (**7**$^+$BAr′F$^-$)$_n$ and (**8**$^+$BAr′F$^-$)$_n$ dissolve in d_8-THF and CD_2Cl_2 to give solutions containing both the monomeric (n = 1) and oligomeric (n > 1) forms. These were unambiguously distinguished via analysis of complexes generated from the isotopically desymmetrized ligand (*R*,*R*)-d_{10}-**1a**, Scheme 2. Key to the analysis is that any monomeric complexes (n = 1) in which ligand **1** is P,P-chelating can only be generated as d_{10}-isotopologues (one ArP(C$_6$D$_5$)$_2$ and one ArP(C$_6$H$_5$)$_2$ coordinate to the Pd). In contrast, any species generated by ligand **1** acting as a bis-monodentate P-ligand, to generate oligomeric rings or chains, must generate a statistical 1:2:1 ratio of $d_0/d_{10}/d_{20}$ isotopologues at the Pd centers in the oligomer, Figure 3. The ^{31}P nucleus in the P(C$_6$D$_5$)$_2$ moiety experiences a ca. −0.5 ppm net isotope shift upfield of that in the P(C$_6$H$_5$)$_2$ moiety, and consequently the isotopologues are readily distinguished by analysis of $^2J_{PP}$ patterns in the ^{31}P^{31}PCOSY (see Supporting Information).

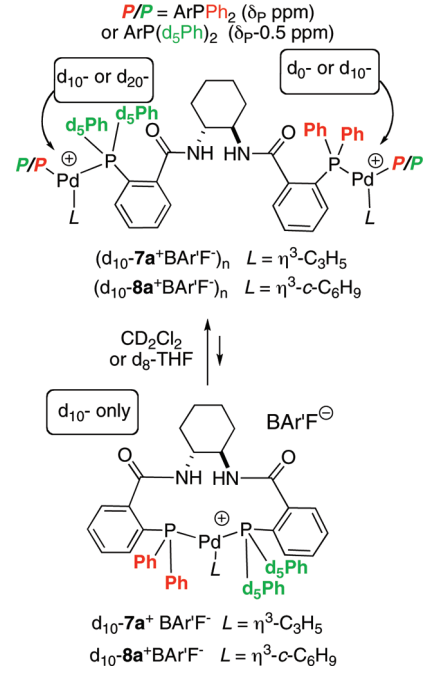

Figure 3. Use of isotopically desymmetrized ligand (*R*,*R*)-d_{10}-**1a** to distinguish monomeric (n = 1) from oligomeric (n > 1) forms of Pd complexes (d_{10}-**7a**$^+$BAr′F$^-$)$_n$ and (d_{10}-**8a**$^+$BAr′F$^-$)$_n$ via ^{31}P^{31}PCOSY.

Monomeric η^3-Allylic Complex 7$^+$BAr′F$^-$. ^{31}P{^{1}H} NMR analysis of the concentration-dependence of the monomer−oligomer distribution in (**7**$^+$BAr′F$^-$)$_n$, showed that below a threshold [Pd]$_{TOTAL}$ concentration of 23 mM in CD_2Cl_2, the solution became sufficiently free of oligomers[16] (<5%), to allow detailed analysis of the monomeric complex **7**$^+$ by ^{1}H, ^{13}C, and ^{31}P NMR. On complexation to the (η^3-C$_3$H$_5$)Pd cation the two phosphine groups in ligand **1** become inequivalent and an 'AB' spin system ($^{2Pd}J_{PP}$) will be generated in the ^{31}P{^{1}H} NMR spectrum. If the ligand maintains a time-average C_2-symmetry, then the two 180° related orientations of the allyl group (formally 'rotamers') results in a degenerate pair of complexes, and while interconversion will result in exchange of P_A and P_B nuclei, a single complex should be observed. However, the ^{31}P{^{1}H} NMR spectrum contains two distinct monomeric species (*exo*-**7**$^+$ and *endo*-**7**$^+$, both with J_{PP} = 35 Hz), present in equal ratio (K = 1.0), showing that, at the NMR time scale, the conformation of **1** in the 13-membered chelate does not have C_2-symmetry. A combination of ^{1}H TOCSY, ^{1}H,^{31}P-HMBC, and ^{1}H,^{13}C-HMQC allowed a complete assignment of the δ- and J-values in the P,P−Pd-η^3-allyl units in the two isomers, Figure 4, and showed that there is no significant difference in allyl structure between isomers and no significant difference in

(32) (a) Brookhart, M.; Grant, B.; Volpe, A. F. *Organometallics* **1992**, *11*, 3920. (b) BAr′F engages in 'very modest but not zero ion pairing', see. (c) Nama, D.; Butti, P.; Pregosin, P. S. *Organometallics* **2007**, *26*, 4942.

(33) (a) Smidt, J.; Hafner, W. *Angew. Chem.* **1959**, *71*, 284. (b) Imaizumi, S.; Matsuhisa, T.; Senda, Y. *J. Organomet. Chem.* **1985**, *280*, 441. (c) Auburn, P. R.; Mackenzie, P. B.; Bosnich, B. *J. Am. Chem. Soc.* **1985**, *107*, 2033.

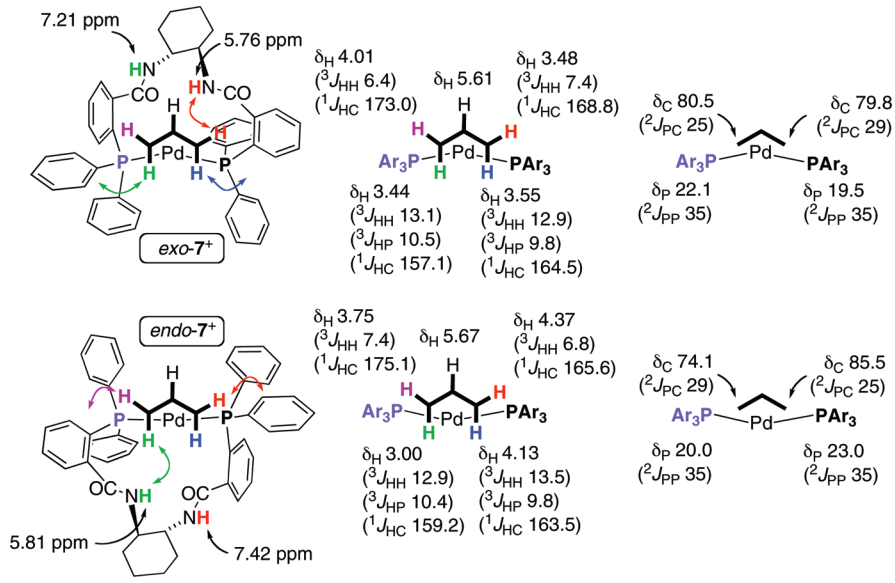

Figure 4. Color-coding showing the static P,P−Pd-η^3-allyl unit during interconversion (k = 2.6(±0.3) s^{-1}, CD_2Cl_2, 25 °C) of monomeric *exo*-**7**$^+$ and *endo*-**7**$^+$ with selected NMR data (δ/ppm, J/Hz) and NOE contacts.

bonding/hybridization between the allyl termini within each isomer. Using 2D EXSY techniques ($^1H^1H$, $^{31}P^{31}P$, and $^{13}C^{13}C$) the two isomers (*exo*-**7**$^+$ and *endo*-**7**$^+$) were found to interconvert via a pathway that preserves the entire set of stereochemical relationships between the nuclei within the P,P−Pd-η^3-allyl unit, see color coding in Figure 4. This striking feature rules out all of the well-known isomerization paths of Pd-allyls (η^1-η^3 interconversion, ligand dissociation, Berry pseudorotation)[34] as these would result in syn/anti exchange of allyl protons and/or cis/trans exchange between allyl termini and the P-donors. The isomerization process must thus involve a conformational change of the ligand **1**, which does not actively involve the P,P−Pd-η^3-allyl unit.

The origins of this conformational change were elucidated by 1D-^{1}H NOE experiments which allowed identification of contacts that were distinct and complementary between the two isomers. Thus in *exo*-**7**, strong correlations were present between one syn allyl proton (red) and one of the two amide protons, and between both anti allyl protons (blue and green) and aromatic protons. In contrast, correlations in *endo*-**7** were present between one anti allyl proton (green) at the opposite allyl terminus and one of the two amide protons, and between both syn allyl protons (magenta and red) and unspecified aromatic protons. In both isomers, there is a ca. 1.5 ppm difference in chemical shifts between the two amide protons and in both cases the NOE contacts to the allyl protons are from the higher field NH protons (ca. 5.8 ppm), which shift to a lower field environment (ca. 7.3 ppm) on isomer interconversion. The only explanation that accounts for all of the above NMR data is that the ligand conformation results in a shallow curved surface being formed around the Pd-allyl moiety, with one amide NH (ca. 5.8 ppm) on the concave surface, and the other on the convex surface; isomerization then involves inversion of the conformation such that the concave surface becomes the convex, and vice versa.

Monomeric η^3-Cyclohexenyl Complex 8$^+$BAr′F$^-$. Analogous $^{31}P\{^1H\}$ NMR studies conducted with the η^3-cyclohexenyl complex (**8**$^+$BAr′F$^-$)$_n$ revealed two distinct differences to (**7**$^+$BAr′F$^-$)$_n$. First, there was a far higher propensity for oligomerization,[22] resulting in much lower concentration samples being required to obtain oligomer-free solutions of **8**$^+$ (4.2 mM in CD_2Cl_2, or 2.0 mM in d_8-THF). Second, instead of there being two isomers present (cf. *exo*/*endo*-**7**$^+$), a single AB system ($^{2Pd}J_{PP}$ = 34 Hz) was apparent in the $^{31}P\{^1H\}$ NMR spectrum, with no evidence for resolution into two species, even on cooling to −50 °C.

Detailed analysis of the ^{1}H NMR spectrum of [**8**]$^+$[BAr′F]$^-$ proved challenging. There was substantial signal overlap (there are 40 aryl CH protons, including BAr′F, in the range δ_H 6.6−7.7 ppm and 14 aliphatic protons in the range δ_H 1.2−2.2 ppm), as well as rapid $T_{1,2}$ relaxation, which rendered 1D TOCSY, 2D HSQC, and HBMC experiments uninformative and thwarted extraction of H,H coupling constants. Nonetheless, 2D COSY, TOCSY, and NOESY analyses, assisted by ^{2}H-labeled complexes (Scheme 3), allowed assignment of the chemical shifts of the cyclohexenyl moiety, the ligand scaffold and a partial assignment of the aromatic protons (see Supporting Information for full details). As with **7**$^+$, the ^{1}H NOESY and amide chemical shift data was indicative of a curved ligand surface. The central allylic proton (red in Figure 5) has an NOE contact to the C(H)N unit in the cyclohexane scaffold (ring **C**), the chemical shift of the adjacent amide proton (7.09 ppm) indicates that this methine proton (C(H)N) is on the concave surface of the complexed ligand. Three of the four protons on methylene groups adjacent to the allyl termini in the η^3-

(34) See for example: (a) Vrieze, K. In *Dynamic Nuclear Magnetic Resonance Spectroscopy*; Jackman, L. M., Cotton, F. A., Eds.; Academic Press: New York, 1975. (b) Albinati, A.; Kunz, R. W.; Ammann, C. J.; Pregosin, P. S. *Organometallics* **1991**, *10*, 1800. (c) Hansson, S.; Norrby, P.-O.; Sjögren, M.; Åkermark, B.; Cucciolito, M. E.; Giordano, F.; Vitagliano, A. *Organometallics* **1993**, *12*, 4940. (d) Breutel, C.; Pregosin, P. S.; Salzmann, R.; Togni, A. *J. Am. Chem. Soc.* **1994**, *116*, 4067. (e) Gogoll, A.; Örnebro, J.; Grennberg, H.; Bäckvall, J.-E. *J. Am. Chem. Soc.* **1994**, *116*, 3631. (f) Pregosin, P. S.; Salzmann, R.; Togni, A. *Organometallics* **1995**, *14*, 842. (g) Malet, R.; Moreno-Mañas, M.; Parella, T.; Pleixats, R. *J. Org. Chem.* **1996**, *61*, 758. (h) Ramdeehul, S.; Barloy, L.; Osborn, J. A.; De Cian, A.; Fischer, J. *Organometallics* **1996**, *15*, 5442. (i) Boog-Wick, K.; Pregosin, P. S.; Trabesinger, G. *Organometallics* **1998**, *17*, 3254. (j) Gogoll, A.; Grennberg, H.; Axén, A. *Organometallics* **1998**, *17*, 5248. (k) Solin, N.; Szabó, K. J. *Organometallics* **2001**, *20*, 5464.

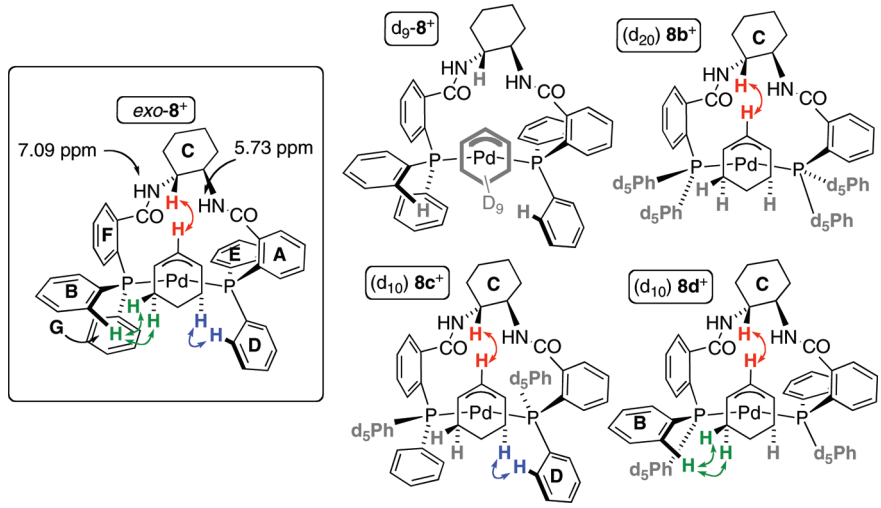

Figure 5. Key NOE contacts for *exo*-**8**$^+$, d_9-**8**$^+$, (d_{20})-**8b**$^+$, (d_{10})-**8c**$^+$, and (d_{10})-**8d**$^+$ where gray indicates a deuterated moiety and associated absence of NOE. Note that all ortho protons experience time-average NOE contact. See Supporting Information for 2D NOESY data.

cyclohexenyl rings display NOE contacts (blue and green in Figure 5) to aryl rings.

The aryl rings exhibiting NOE contacts with the η^3-cyclohexenyl ring were identified as simple Ph groups (rings **B**, **D**, **E**, or **G**) by the absence of these NOE contacts in the perdeuterophenyl complex (d_{20})-**8b**$^+$. The use of the d_9-**8** complex in which the η^3-cyclohexenyl ring is perdeuterated confirmed that the NOE contacts with the Ph rings are from methylene groups in the η^3-cyclohexenyl ring, rather than methylenes in the cyclohexane ligand scaffold (ring **C**). The triangulating set of contacts (red, blue, and green in Figure 5) indicate that the orientation of the η^3-cyclohexenyl ring is analogous to *exo*-**7**$^+$, identifying the single species observed for [**8**]$^+$[BAr'F]$^-$ as *exo*-**8**$^+$. Since the two isomers of the simple allyl complexes *exo*/*endo*-**7**$^+$ are isoenergetic, there must be a substantial destabilization in *endo*-**8**$^+$ caused by the allyl unit being substituted at one or both anti positions. Computational studies, vide infra, identified this destabilization as arising from steric strain being induced in *endo*-**8**$^+$ by clash of the ligand scaffold (ring **C**) with the two methylene units at the allyl termini in the η^3-cyclohexenyl ring.

The orientation of the phenyl rings in the Ph_2P units was explored by way of comparison of the 2D ^{1}H NOESY data of unlabeled complex **8**$^+$ with that obtained for diastereoisotopomeric complexes (d_{10})-**8c**$^+$ and (d_{10})-**8d**$^+$, Figure 5. With (R_P,R_P)-based ligand **1c**, the NOE between the methylene group at the *pro-R* allyl terminus in (d_{10})-**8c**$^+$ was absent, clearly identifying the NOE (green protons) in *exo*-**8**$^+$ as arising from phenyl ring **B** bisecting the methylene group. Analogously, with (S_P,S_P)-based ligand **1d**, the NOE between the pseudo-axial proton on the methylene group at the *pro-S* allyl terminus in (d_{10})-**8d**$^+$ was absent, identifying this NOE (blue protons) in *exo*-**8**$^+$ as arising from proximity to phenyl ring **D**.

Computational Investigation of Complexes 7$^+$ and 8$^+$. The structures of the Pd complexes **7**$^+$ and **8**$^+$ pose nontrivial computational problems. Ligand **1** is large and flexible, necessitating a thorough and unbiased search of several thousand plausible conformations. On the other hand, transition metal complexes in general require advanced quantum chemical methods in order to obtain structures and energies with an accuracy that is sufficient to allow meaningful comparisons to solution NMR data. Today, the methods of choice are usually hybrid DFT methods, like B3LYP.[35] Such calculations are time-consuming, requiring days for each optimized geometry with complexes of the current size. To circumvent this problem, fast molecular mechanics (MM) methods can be utilized for the conformational searches, and only the most promising structures are then subjected to more rigorous DFT investigations. For this approach to be successful, the MM method must be reliable; use of "off the shelf" unvalidated MM is *not* recommended for metal complexes. In the current work, we do all conformational searches with a modified MM method that has previously been found to have good accuracy for (η^3-allyl)Pd complexes.[36] Final energies come from DFT optimizations in solvent, as described in the Computational Methods section. Structures **7**$^+$ and **8**$^+$ yielded very similar results, except that for **7**$^+$, there was very little difference between *endo* and *exo* structures in terms of the number of conformations found or their energies, whereas for **8**$^+$, endo structures were significantly fewer and higher in energy. The conformational ensemble for **8**$^+$ up to 18 kJ mol^{-1} above the global minimum is depicted in Figure 6. The corresponding ensembles for **7**$^+$ can be visualized as taking the exo ensemble for **8**$^+$ and inserting either an *exo*- or *endo*-η^3-allyl moiety in place of the *exo*-η^3-cyclohexenyl. It can be seen that all low energy conformations are remarkably similar, folding the backbone cyclohexane into close proximity with the Pd-allyl moiety. Only two conformations in this energy range display a fold with the backbone endo to the η^3-cyclohexenyl unit. The only other major difference between the different folds is in the orientation of one of the amide units. For several conformations, the amide N−H is pointing into the concave embrasure, close to one allyl terminus (yellow hydrogen in Figure 6), whereas for the others, only carbonyl oxygens are pointing inward toward the Pd-allyl moiety. It can also be seen that for the *endo* conformations, the amide units are far from the reactive allyl termini. Other, more minor differences arise from the orientations of the phenyl groups combined with minor rotation around the Pd−P bonds. Interestingly, one side of the η^3-cyclohexenyl moiety interacts mainly with a backbone

(35) (a) Lee, C.; Yang, W.; Parr, R. G. *Phys. Rev. B* **1988**, *37*, 785. (b) Becke, A. D. *J. Chem. Phys.* **1993**, *98*, 5648. (c) Stephens, P. J.; Devlin, F. J.; Chabalowski, C. F.; Frisch, M. J. *J. Phys. Chem.* **1994**, *98*, 11623.

(36) Hagelin, H.; Åkermark, B.; Norrby, P.-O. *Organometallics* **1999**, *18*, 2884.

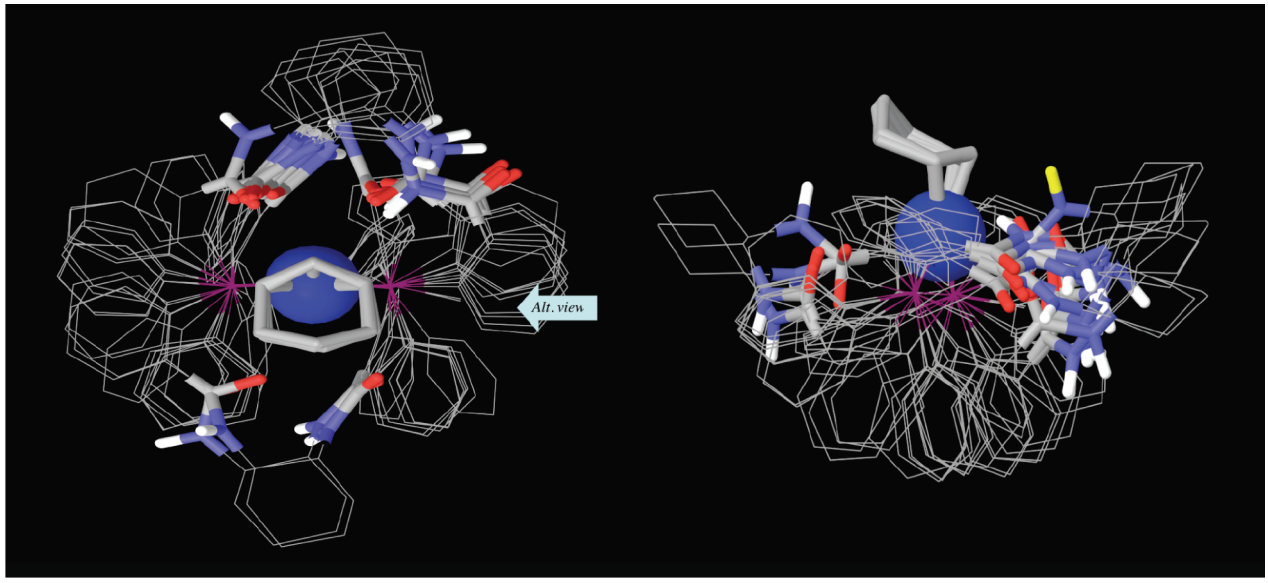

Figure 6. Two views of the MM conformational ensemble of $\mathbf{8}^+$, up to 18 kJ mol^{-1}. C−H hydrogens are hidden, the η^3-cyclohexenyl and amide moieties are shown as tubes, and Pd in CPK style. Left hand image 'front view'; right-hand image 'side view' of $\mathbf{8}^+$, see arrow in 'front view'. In the 'side view' the favored conformer has an amide hydrogen (yellow) close to the *pro-S* allyl terminus.

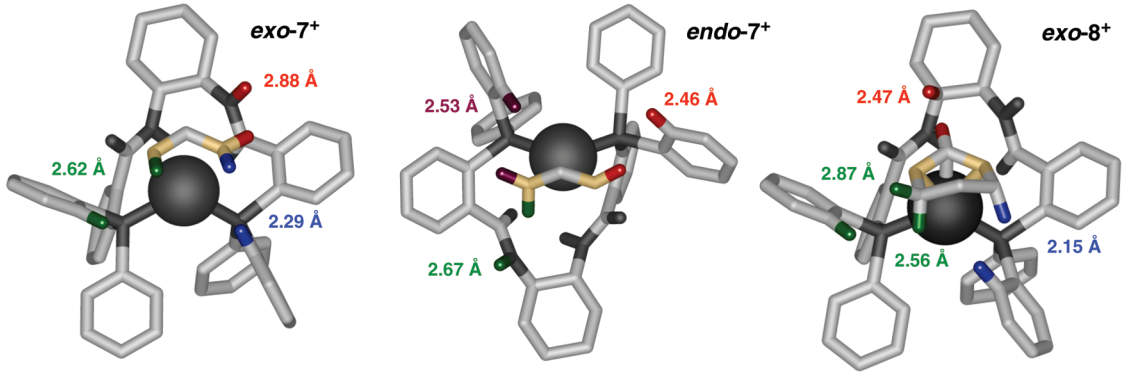

Figure 7. DFT-optimized lowest energy conformers for *exo*-$\mathbf{7}^+$, *endo*-$\mathbf{7}^+$ and *exo*-$\mathbf{8}^+$. Key NOE contacts color coded as in Figures 4 and 5. Allyl termini are highlighted in pale orange. All heteroatoms (O, N, Pd, P) are colored dark gray.

benzene, not the pendant phenyl groups, in most low energy conformers. Attempts to enforce ligand C_2-symmetry or any geometry where the four pendant phenyl groups are close enough to the η^3-allyl moiety to give a structure with any resemblance to that in Figure 2, results in steric energies more than 100 kJ mol^{-1} above the global minimum. Earlier rationalizations of selectivities with ligand **1** have predominantly been built on the assumption that it is the pendant phenyl groups that interact with the η^3-allyl moiety or the nucleophile.[20] The structures determined in the current work indicate that additional control mechanisms are active.

The lowest energy conformations of both $\mathbf{7}^+$ and $\mathbf{8}^+$ were optimized using DFT, as described in the Computational Methods section, validating the gross structural features and energy ranking of the MM conformations. The most populated conformations were used to map expected NOE contacts.[37] Comparison of these maps to the NOESY data showed excellent agreement (Figure 7) reinforcing the assignment of the experimental structures.

Alkylation of Complex *exo*-$\mathbf{8}^+$. To ensure that our structural studies on the isolated complex *exo*-$\mathbf{8}^+$ were pertinent to the catalytic reaction, and specifically to the selectivity for delivery of malonate to the *pro-S* carbon of the η^3-cyclohexenyl ring to generate (*S*)-**6**, we reacted malonate nucleophile (CHE_2) with *monomeric* [$\mathbf{8}^+$][BAr′F] in THF and measured the ee of the alkylkation product **6** by chiral HPLC,[38] 'ee obs', Table 1. These stoichiometric reactions were conducted with a range of escort ions (M^+) to the malonate nucleophile and gave selectivities that perfectly matched the trend reported for the catalytic reaction[4,9] (Figure 2). Thus with Li^+ (Table 1, entry 1) near-racemic cyclohexenyl malonate **6** was obtained and the selectivity increased progressively as M^+ was changed from Li to Na, K and Cs (Table 1, entries 1, 2, 7, and 8). With Bu_4N^+ as escort ion, (*S*)-**6** was obtained in very high ee (entry 9).

Stoichiometric reaction of $NaCHE_2$ or Bu_4NCHE_2 with *oligomeric* ([$\mathbf{8}^+$][BAr′F])$_n$ in which ca. 93% of (*R,R*)-**1** is complexed in a binuclear *nonchelate* mode, gave **6** with low selectivity (entries 4 and 10), the sense of induction actually being slightly reversed with Na as escort ion, in both cases confirming that catalytic flux via the monomer ($\mathbf{8}^+$) is essential for attaining high selectivity.

(37) Hagelin, H.; Åkermark, B.; Norrby, P.-O. *Chem.—Eur. J.* **1999**, *5*, 902.

(38) The use of dibenzyl malonate, rather than dimethyl malonate, facilitates reliable chiral HPLC separation of the enantiomers of **6** (E = CO_2Bn), see: (a) Trost, B. M.; Radinov, R. *J. Am. Chem. Soc.* **1997**, *119*, 5962.

Table 1. Enantiomeric Excesses (ee's) in Stoichiometric[a] Alkylation of Monomeric[b] [**8**$^+$] with Excess [$MCHE_2$] (M = Li, Na, K, Cs, Bu_4N; E = CO_2Bn) to Give (*S*)-**6**, Compared to the Selectivity Predicted by DFT Calculations

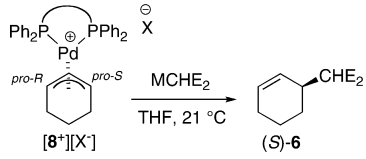

entry	M^+	X-	ee obs[c]	ee calcd[d]
1	Li	BAr′F	3	−16
2	Na	BAr′F	44 (49)[a]	67
3[e]	Na[e]	BAr′F	85	–
4[f]	Na	BAr′F	−16[f]	–
5	Na	OTf	83 (83)[a]	–
6	Na	Cl	93 (87)[a]	–
7	K	BAr′F	76	84
8	Cs	BAr′F	89	>99
9	Bu_4N	BAr′F	98[g] (95)[a]	>99
10[f]	Bu_4N	BAr′F	6[f]	–
11	Bu_4N	OTf	90 (94)[a]	–
12	Bu_4N	Cl	92 (95)[a]	–

[a] Values in parentheses are for *catalytic* alkylations employing 2.5 mol % [**8**$^+$][X] (1.0 mM) and (*S*)-cyclohexenyl acetate. [b] [**8**$^+$][BAr′F], 1.0 mM, >95% monomeric. For [**8**$^+$][OTf] and [**8**$^+$][Cl] (prepared in situ from **13/15**$^+$[OTf$^-$] and (*R*,*R*)-**1**) some oligomer is present. [c] ee of (*S*)-**6** by chiral HPLC on AD-H column. [d] ee of (*S*)-**6** calculated from DFT-derived ΔE between TS for addition of $MCHE_2$ to *exo*-**8**$^+$. [e] 20% Bu_4N, 80% Na. [f] Stoichiometric reaction employing 27 mM [**8**$^+$][BAr′F] (7% monomeric). [g] Analogous reactions conducted after pre-equilibration of 1 mM [**8**$^+$][BAr′F] with 100 mM MeOL (L = H or D) in THF (^{1}H NMR analysis shows full exchange NH to NL in [**8**$^+$][BAr′F]) gave identical enantioselectivity, within experimental error (four runs with L = H, four runs with L = D).

Addition of *catalytic* (20 mol %) Bu_4NCHE_2 to the reaction of $NaCHE_2$ with [**8**$^+$][BAr′F] raised the selectivity for (*S*)-**6** substantially (compare entries 2 and 3), suggesting at least a ca. 3-fold selectivity for attack by Bu_4NCHE_2,[39] which can be regenerated via equilibrium: $[Bu_4N][BAr'F] + NaCHE_2 \rightarrow Bu_4NCHE_2 + NaBAr'F$.[5] With the concept that greater dissociation of the nucleophile from the escort-ion (M^+) is a key component for facilitating a monomer-specific *activated* pathway that increases *pro-S* selectivity, we compared the effect of X^-, the counterion to the Pd complex (X = BAr′F, OTf, Cl), on reactions involving Na^+ and Bu_4N^+ escort ions. Consistent with this concept of dissociation, increasing the strength of the interaction between Na^+ and X^-, so as to increase the dissociation of the Na^+ from the CHE_2 anion, gave a substantial rise in selectivity (compare entries 2, 5, and 6), despite the increase in oligomer concentration due to the change from X = BAr′F to OTf and Cl. Moreover, with the Bu_4N^+ escort-ion, which interacts less strongly, there was little effect (compare entries 9, 11, and 12).[39]

When [**8**$^+$][X] was used as a *catalyst* for the reaction of cyclohexenyl acetate (**5**),[40] the selectivities (ee values in parentheses in entries 2, 5, 6, 9, 11, and 12 in Table 1) were very similar to those obtained in the stoichiometric reactions. For the reactions involving $NaCHE_2$ (entries 2, 5 and 6) this initially appears to contradict the above conclusions, as under *catalytic* conditions X should be an acetate ion. However, we have previously shown that *catalytic* NaBAr′F (which will be generated from $NaCHE_2$ + [**8**$^+$][BAr′F]) is highly efficient at abstracting acetate ion from Pd-(allyl)OAc complexes,[5] in this case continually regenerating [**8**$^+$][BAr′F]. Consistent with this conclusion, for reactions with the Bu_4N^+ escort-ion, the nature of X (BAr′F, OTf, Cl, or AcO) does not impact significantly on the selectivity (entries 9, 11, and 12).

Earlier rationales for selectivity in the alkylation of cycloalkenyl esters (Figure 2) were based on steric deactivation of the nucleophile by phenyl rings.[20] As is evident from the NMR and computational data outlined above, in no case can any of these rings reach past the allyl moiety to influence the incoming nucleophile. Any influence of these substituents on the reaction selectivity would be expected to come from induced torqueselectivity[41] caused by specific interactions with the η^3-cyclohexenyl moiety. The DFT-optimized structure for *exo*-**8**$^+$ shows the closest phenyl ring to the η^3-cyclohexenyl ring to be ring **B** in Figure 5, which gives rise to the NOE contacts highlighted in green in Figure 7. This interaction causes a slight rotation of η^3-cyclohexenyl ring (anticlockwise when viewed with the η^3-C_6H_9 moiety in front of the Pd) such that one allyl terminus is located slightly above and the other slightly below the formal square plane around Pd, see central structure in Figure 8. On its own, this induced torqueselectivity[41] will favor nucleophilic attack of malonate anion (CHE_2) at the *pro-R* terminus as this leads to continued anticlockwise rotation of the η^3-cyclohexenyl ring during formation of the new C−C bond in the nascent η^2-bound product (*R*)-**6**. However, this (*R*)-selectivity is *opposite* to that observed under the catalytic[9,42] and stoichiometric conditions (Figure 2 and Table 1), where (*S*)-selectivity ranges from near-racemic to near-perfect, depending on the identity of the 'escort-ion' to the nucleophile (M^+) and, in some cases the identity of X^-, Table 1.

To investigate the underlying causes for the above selectivity trend, we located approximate transition states for addition of malonates with a range of escort ions to *exo*-**8**$^+$. As discussed in the Computational Methods section, a continuum solvation model is both necessary and sufficient for accurate location of these very polar transition states. From the studies above, we considered the common computational practice of excluding the counterion to *exo*-**8**$^+$ from the calculations, but the malonate escort ion M^+ must be included since one of the goals of the

(39) Madec, M.; Prestat, G.; Martini, E.; Fristrup, P.; Poli, G.; Norrby, P.-O. *Org. Lett.* **2005**, *7*, 995.

(40) To avoid complications arising from the memory effects that are known to attend these reactions under some conditions (see ref 10), we analysed the enantiomeric excess of **6** after ca. 10 turnovers, at which point the conversion of cyclohexenyl acetate (**5**) is ≤50% after which turnover rate drops precipitously. In this manner, the powerful kinetic resolution for this process leads to selective study of the outcome of generation and attack on [**8**$^+$][OAc$^-$] via the *matched manifold* involving (*S*)-**5**. For reactions involving Bu_4N as escort ion, subsequent slow turnover via the mismatched manifold proceeded without drop in selectivity. In contrast, and as expected,[10] with reactions involving Na^+ as the escort ion, the selectivity dropped after the onset of turnover via the mismatched manifold.

(41) Induced rotation of the allyl moiety can have a major influence on the relative reactivity of the two allyl termini: Oslob, J. D.; Åkermark, B.; Helquist, P.; Norrby, P.-O. *Organometallics* **1997**, *16*, 3015.

(42) For cyclopentenyl substrates the same trend in M^+ is observed, except that reaction with $LiCHE_2$ gives rise to the opposite enantiomer of product in moderate selectivity (ca. 40% ee *R*; see ref 19). Due to the propensity of Pd η^3-cyclopentenyl species to undergo β-H elimination to generate cyclopentadiene (see: (a) Fairlamb, I. J. S.; Lloyd-Jones, G. C.; Vyskočil, S.; Kočovský, P. *Chem. Eur. J.* **2002**, *8*, 4443.) We have only studied the η^3-cyclohexenyl complexes. However, the mechanistic rationale presented herein is fully consistent with the results obtained with η^3-cyclopentenyl substrates under catalytic conditions. The difference between the two systems is simply that the 'crossing point' where the net selectivity for *pro-R* attack by CHE_2 begins to dominate over *pro-S* attack is at M = Li for η^3-cyclohexenyl, but between M = Li/Na for η^3-cyclopentenyl.

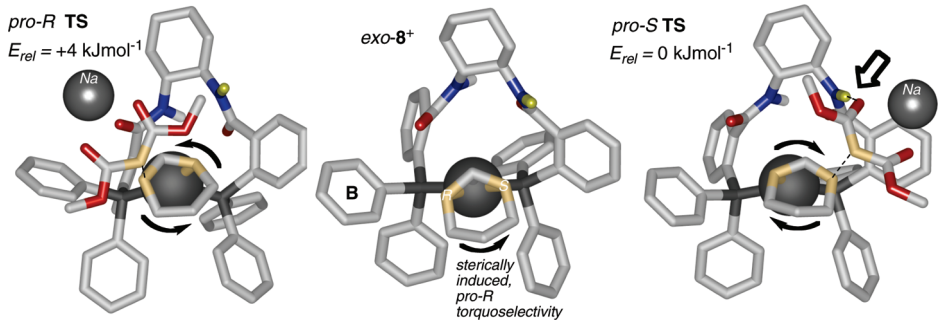

Figure 8. (Center) DFT-optimized structure of *exo*-**8**$^+$, with allyl termini highlighted in pale orange. The induced (ring **B**) *pro-R* (anticlockwise) torquoselectivity is indicated with arrow. (Outer Images) DFT-optimized transition states (TSs) for *pro-R* and *pro-S* addition of $NaCHE_2$. The attacking central carbon of malonate is highlighted in pale orange, resulting torquoselection with curved arrow, and the key enolate-amide hydrogen bond with a bold arrow.

current study is to reproduce the selectivity-trend in Table 1. We utilized the global minimum energy conformation of *exo*-**8**$^+$ together with a malonate chelating with both carbonyl oxygens to the escort ion (M^+).[39,43] This still left three possible staggered approaches of the malonate to each allyl terminus. Very interestingly, with most escort ions, one TS had a substantially lower energy than any alternative approach, illustrated for the Na^+ malonate in Figure 8.[44] In this *pro-S* TS, leading to the experimentally observed (*S*)-**6**, we find a strong hydrogen bond between one malonate enolate-oxygen and the amide hydrogen (highlighted with arrow in Figure 8). Simultaneously, the escort ion gains some stability from an interaction with the proximal backbone benzene moiety. Likewise, for some *pro-R* TSs, the escort ion could gain stability by a long-range dipole-ion interaction with the amide carbonyl pointing into the concave face (Figure 6) in close proximity to the allyl terminus. In calculations without the continuum solvation model (gas phase), which are not discussed further, this interaction becomes a strongly exaggerated coordination.

For weakly coordinating escort ions like Cs^+, the hydrogen bond interaction dominated, favoring the pro-*S* TS by ca. 22 kJ mol^{-1} in THF (18 kJ mol^{-1} in CH_2Cl_2).[45] As discussed in the Computational Methods section, the magnitude of this selectivity is exaggerated due to the missing vibrational entropy, which in reality must favor the looser pro-*R* TS; the experimental selectivity (ee obs, Table 1) corresponds to a free energy difference of ca. 8 kJ mol^{-1}, although this value itself is compromised by some competing low-selectivity reaction occurring via the oligomer. Using more strongly coordinating escort ions will attenuate the hydrogen bond and at the same time increase the importance of the amide carbonyl interaction, so that for Li^+, the calculated difference between the two paths is less than 1 kJ mol^{-1}, in perfect agreement with the result shown in Table 1, entry 1. Such a good agreement is surely fortuitous; due to the problem of intersecting continuum cavities at the TS, we see apparently random energy variations of a few kJ mol^{-1} between virtually identical structures. However, the trend itself is not sensitive to these small variations, and it matches well the experimental trend: compare ee obs and ee calcd values for entries 1, 2, 7, 8, and 9, in Table 1. We note that H-bond mediated delivery of the nuclophile requires that it possess a strongly negative hydrogen bond acceptor, in a 1,3-relationship to the reactive (nucleophilic) site. This feature, present in for example carboxylates, 1,3-dicarbonyls, carbonates,[46] or phthalimides, is found in nearly all known cases where ligand (*R*,*R*)-**1** leads to high selectivity for attack at the *pro-S* allyl terminus, or corresponding position in analogous cyclic intermediates.[20] We also note that the energy difference between *endo*-**8**$^+$ and *exo*-**8**$^+$ is not a requirement for high selectivity with cycloalkenyl substrates. In the *endo* isomer, the cycloalkenyl ring will block delivery of the nucleophile to the *pro-R* allyl terminus via the amide hydrogen-bond route and therefore the reaction will be funneled through the exo isomer, provided that the conformational exchange is fast relative to nucleophilic attack.[45] Moreoever, in 2-substituted cycloalkenyl substrates, which will generate η^3-intermediates analogous to **8**$^+$ but with a substituent at the central allyl carbon, the amide-H-bond mediated delivery of the nucleophile will encounter steric strain in both the *exo* and *endo* isomers, while for open-chain allylic substrates, H-bond mediated delivery of the nuclophile is not strained for either isomer. Both factors may help to rationalize the lower selectivities that are obtained with these types of substrates.[20]

It was recently shown that Pd complexes of (*R*,*R*-**1**) and analogues retain high selectivity in the catalyzed reaction of cycloalkenyl and simple linear allyl esters with "hard" nucleophiles, such as lithium or tin enolates,[7] and lithium methylpyridine trifluoroborates.[8] Under such strongly basic conditions, ligand N−H deprotonation would lead to enhanced interaction of the carbonyl with the escort ion M^+ (Li, Sn), thus augmenting selectivity *via* this pathway.[47]

Generation of Complex *exo*-8$^+$ from Cyclohexenyl Esters. Ligand **1** is known for a dual mode of reactivity; not only will it induce a high selectivity in nucleophilic attack on cycloalkenyl substrates, but it also achieves powerful kinetic resolution of chiral substrates and is able to efficiently desymmetrize meso

(43) (a) Norrby, P.-O.; Mader, M. M.; Vitale, M.; Prestat, G.; Poli, G. *Organometallics* **2003**, *22*, 1849. (b) Svensen, N.; Fristrup, P.; Tanner, D.; Norrby, P.-O. *Adv. Synth. Catal.* **2007**, *349*, 2631. (c) Fristrup, P.; Ahlquist, M.; Tanner, D.; Norrby, P.-O. *J. Phys. Chem. A* **2008**, *112*, 12862.

(44) Due to the stabilization provided by the continuum model, it was also possible to find completely "open approaches" without interaction with any ligand moiety. These open approaches were insignificant for *pro*-S attack where these had a higher energy than the amide H-bonded transition states. For *pro-R* attack, these open approaches were more prevalent and it was necessary in all cases to locate both types of transition states and compare their energies.

(45) Higher enantioselectivity is obtained in CH_2Cl_2 versus THF under catalytic conditions (see ref 9). This may arise from a combination of factors, including less oligomerization of **8**$^+$ and lower $MCHE_2$ concentration in CH_2Cl_2, the latter allowing more efficient equilibration of oligomeric **8**$^+$/*endo* monomeric **8**$^+$ with *exo*-**8**$^+$ relative to nucleophilic attack.

(46) For the use of $[HCO_3]^-$ as nucleophile for the asymmetric 'hydrolysis' of cycloalkenyl esters to the corresponding alcohols, via decarboxylation of an intermediate cycloalkenyl hydrogen carbonate ester, see. (a) Lüssem, B. J.; Gais, H.-J. *J. Am. Chem. Soc.* **2003**, *125*, 6066.

substrates.Thus, in the presence of Pd(*R*,*R*)-**1**, (*S*)-cyclohexenyl acetate **5** reacts up to 2 orders of magnitude faster than the (*R*)-enantiomer,[11] and in the meso-forms of 3,6-X_2-cyclohexene (X = carboxylate leaving groups such as ester, carbonate, *N*-tosyl carbamate,), it is the X group on the (*S*)-configured allylic carbon that is expelled with very high selectivity.[20] The carboxylate ionization is the microscopic reverse of nucleophilic attack on the (η^3-allyl)Pd complex; in fact, the reaction is reversible[5,48] and Pd(*R*,*R*)-**1** catalyzed substitution of, e.g., trichloroethyl carbonate by benzoate proceeds with very high selectivity.[20] The same type of computational approach can be applied here as was used for the nucleophilic attack. One major difference is that the overall system is net neutral and ionogenic: the two neutral fragments Pd(*R*,*R*-**1**) and (*R*)-**5**/(*S*)-**5** react to give *exo*-**8**$^+$ and an acetate anion, making the use of the continuum model absolutely essential.[37]

Looking first at the neutral preionization η^2-allyl ester complexes, we can see that already in the ground state, the acetate carbonyl of (*S*)-**5** accepts a hydrogen bond from the amide hydrogen on the concave side of **1**, whereas no corresponding stabilization is available for (*R*)-**5**. The hydrogen bond stabilizes the [η^2-(*S*)-**5**]Pd(**1**) complex by 14 kJ mol^{-1} relative to the [η^2-(*R*)-**5**]Pd(**1**) diastereomer. Upon ionization, this energy difference increases due to the increased negative charge on the acetate, until at the TS, Figure 9, we calculate an energy difference of 38 kJ mol^{-1} between the isomers. As was the case with nucleophilic attack, vide supra, this energy difference is exaggerated by our neglect of entropic contributions; the experimental selectivity corresponds to a free energy difference that is about half of what we calculate. *meso*-3,6-Diacetoxycyclohexene gives results that are entirely consistent with those from monoacetate **5**. Upon generation of the neutral preionization η^2-allyl diester complex, only one of the two enantiotopic acetate groups can engage in hydrogen bonding to the amide; this acetate will be selectively ionized, due to the stabilization of the leaving acetate anion through hydrogen bonding.

3. Summary

By exploiting the concentration-dependency and reversibility of the oligomerization, in concert with the exceptionally low interactivity of the B[(3,5-$(CF_3)_2C_6H_3)_4$]$^-$ anion ("BAr′F")[33] with Pd-allyl cations,[5] we have prepared monomeric cationic complexes [(η^3-C_3H_5)Pd(*R*,*R*)-**1**]$^+$ (**7**$^+$, two isomers: *exo*/*endo*) and [(η^3-*c*-C_6H_9)Pd(*R*,*R*)-**1**]$^+$(**8**$^+$, single isomer: *exo*) that are sufficiently free of oligomer to permit their detailed study by ^{1}H, ^{13}C, and ^{31}P NMR spectroscopy. Employing deuterium labeling (Chart 3, Schemes 2 and 3), the complexes were shown to exist as monomeric *chelates* (Figure 3) with structures that could be partially eluciated by a study of NOE contacts (Figures 4 and 5). Monomeric complex *exo*-**8**$^+$ was shown to react with malonate nucleophile ($MCHE_2$) to give the cyclohexenyl malonate (*S*)-**6** in up to 98% ee, depending on the identity of M$^+$ and, in some cases, X$^-$ (ee obs, Table 1) in excellent agreement with Pd(*R*,*R*)-**1** catalyzed reactions involving cyclohexenyl acetate (**5**).[9]

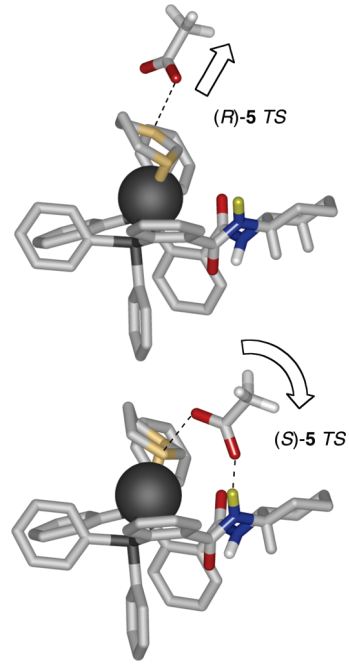

Figure 9. 'Side view' of DFT-optimized TS structures leading to *exo*-**8**$^+$ via ionization of *mismatched* cyclohexenyl acetate (*R*)-**5** (upper) and *matched* cyclohexenyl acetate (*S*)-**5** (lower). The approximate motions of the acetate groups leading to ionization are indicated with arrows.

P,P-Coordination of ligand **1** in **7**$^+$ and **8**$^+$ was then explored computationally, using a modified molecular mechanics method to sift out favored conformers of the very flexible 13-membered chelate, which were then refined by DFT. The outcome was very similar for **7**$^+$ and **8**$^+$, in both cases revealing the 13-membered chelate ring to be puckered such that the backbone cyclohexane is placed in close proximity to the Pd-allyl moiety.[49] There was an excellent correlation between the DFT derived structures and the experimental NOESY data (Figure 7), cross-validating both approaches. The proximity of the amide groups to the Pd center also accounts for the known instability[14,50] of the Pd(0) complexes of **1**.

Nucleophilic attack on *exo*-**8**$^+$ by malonate ($MCHE_2$) was then studied by DFT. For the hypothetical addition of a free malonate anion (no M$^+$), an H-bonding interaction between the enolate oxygen of the malonate and the amide NH on the concave surface of Pd-coordinated (*R*,*R*)-**1** was found to guide the enolate carbon to the proximal (*pro*-*S*) terminus of the η^3-*c*-C_6H_9 unit with perfect selectivity. Introduction of metal counterions resulted in 1,3-dicarbonyl chelation of M$^+$ by the malonate and a resulting attenuation of the H-bonding interaction of the enolate with the amide. Simultaneously, there were

(47) Ligand carbonyl coordination of the Li escort ion in lithium 2-pyridylmethyl trifluoroborate (LiHMDS + methyl pyridine + BF_3) would augment the inherent (*R*)-torquoselectivity for attack in *exo*-**8**. However, with (*R*,*R*)-**1**, *pro*-*S* selectivity still dominates (70 *pro*-*S*/30 *pro*-*R*). Nonetheless, in agreement with the preceding discussion noting the possible interaction of the escort ion with aromatic rings, replacement of the cyclohexane scaffold in (*R*,*R*)-**1** with a 9,10-dihydroanthracene moiety results in highly selective nucleophilic attack at the *pro*-*R* carbon.

(48) (a) Amatore, C.; Jutand, A.; Mensah, L.; Meyer, G.; Fiaud, J.-C.; Legros, J.-Y. *Eur. J. Org. Chem.* **2006**, 1185. (b) Amatore, C.; Gamez, S.; Jutand, A.; Meyer, G.; Moreno-Mañas, M.; Morral, L.; Pleixats, R. *Chem.—Eur. J.* **2000**, *6*, 3372.

(49) A similar coordination geometry and conformation for **1** to that observed for allylic Pd complexes **7** and **8**, is found in the complex Pt(*R*,*R*-**1**)Cl_2 where the Cl centers hydrogen bond to the amide NH groups: (a) Burger, S.; Therrien, B.; Süss-Fink, G. *Acta Crystallogr.* **2004**, *E60*, m1163.

(50) Pd(0) complexes of ligand **1**, and its naphtho analogue, are unstable in solution, losing both amide hydrogens to form two covalent Pd−N bonds, thus generating a neutral, *P*,*P*,*N*,*N*-tetracoordinate mononuclear species. This bright yellow complex is catalytically inactive for allylation reactions and has been characterized by X-ray crystallography (see footnote 11 in ref 18).

increased interactions between the escort ion M^+ and the carbonyl of the amide group proximal to the *pro-R* terminus. Overall, as M^+ became more oxophilic ($Cs^+ \rightarrow Li^+$) this led to a net trend of decreasing attack at the *pro-S* terminus and increasing attack at the *pro-R* terminus to the point where with Li^+ the (*S*)-pathway was virtually isoenergetic with the (*R*)-pathway; the trend in selectivity (ee calcd, Table 1) matching that observed experimentally (ee obs) under both stoichiometric and catalytic conditions.

Analogous studies on the second key part of the catalytic cycle, generation of *exo*-**8**$^+$ from cyclohexenyl acetate (**5**), revealed a fundamental difference in ionization mode between enantiomers of **5**, Figure 9. For the matched substrate (*S*)-**5**, a hydrogen bond from the amide proton on the concave surface to the carbonyl oxygen of the acetate preorients the allyl unit for ionization. This interaction is absent in the less stable (14 kJ mol^{-1}) mismatched pairing with (*R*)-**5** and while not deactivated per se, this process is kinetically noncompetitive with ionization of the matched substrate (*S*)-**5** ($k_S \gg k_R$).[11]

In summary, we have identified that hydrogen-bond interactions of one N−H unit in Pd-coordinated (*R*,*R*)-**1** can substantially accelerate both ionization and nucleophilic attack. This hydrogen-bond directed delivery of the nucleophile has precedent in the elegant design of chiral ferrocene ligands of Hayashi and Ito,[51] although the hydrogen bonding unit appears to be substantially more localized and orientated in Pd(*R*,*R*-**1**) complexes. The interaction provides not only a new rationale for observed selectivities[20,52] but also a design principle for further development of the reaction class.[51] For attack involving harder nucleophiles[7,8,20] with tightly ion-paired escort-ions (M^+) such as Li^+, an alternative selective pathway is available via favorable interaction of M^+ with the carbonyl of the other amide unit. We note that the selectivity mechanism, outlined in cartoon form in Figure 10, differs from most commonly advanced rationalizations in stereoselective synthesis; the high selectivity is obtained by selective favoring of one pathway, not by disfavoring of all undesired paths. Thus, the current reaction is an example of *Ligand Accelerated Catalysis*,[53] and even a rather special case within this class since the acceleration is strongly dependent on the ligand conformation. Only in a chelate will the structure display a concave face with regioselectively placed activating amide groups, thus allowing the desired pathway to out-compete background turnover with poor selectivity by the oligomeric catalysts in the reaction milieu.

NMR Methods. Samples were sealed in NMR tubes (178 mm long, 5 mm diameter) fitted with a Young's valve, under an inert (N_2) atmosphere, using standard Schlenk-line techniques. CD_2Cl_2 was freshly distilled from preactivated 3 Å molecular sieves under an atmosphere of $N_{2(g)}$ prior to use. THF was freshly distilled from Na−benzophenone ketyl under an atmosphere of $N_{2(g)}$ prior to use. [**7**]$^+$[BAr′F]$^-$ (23.5 mg, 13.8×10^{-3} mmol) and [**8**]$^+$[BAr′F]$^-$ (4.2 mg, 2.4×10^{-3} mmol) were dissolved in 0.6 cm^3 CD_2Cl_2 and the resulting 23.0 mM ([**7**]$^+$[BAr′F]$^-$) or 4.0 mM ([**8**]$^+$[BAr′F]$^-$) samples checked for the presence of >95% monomeric chelate by $^{31}P\{^1H\}$ NMR prior to detailed analysis. NMR spectra were recorded on a Varian VNMR 500 spectrometer fitted with Varian 500 H(C/X) PFG or Varian 500 Auto X BM PFG probes. 2D $^1H^1H$ NOESY spectra were generated by employing standard Varian Chempack experiments. Varian Chempack experiments were modified to conduct multinuclear analyses where necessary. See Supporting Information for full details, analysis, and assignments.

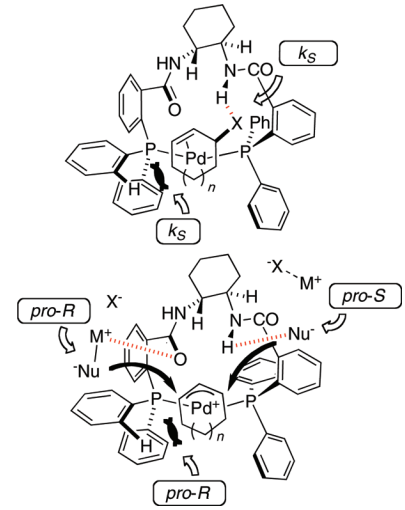

Figure 10. Cartoon model for kinetic resolution (upper graphic) and asymmetric induction (lower-graphic) in the Pd(*R*,*R*)-**1** catalyzed reaction of cyclohexenyl esters with nucleophiles. *pro-R* versus *pro-S* selectivity in nucleophilic attack depends identity of escort ion M^+, counterion X^-, and availability of a hydrogen bond acceptor, in a 1,3-relationship to the nucleophilic site (e.g., malonate, phathalimide, carboxylate, carbonate, etc.).

Computational Methods. Using in-house parametrization methods,[54] we have earlier developed MM3* force fields[55] specifically for (η^3-allyl)Pd complexes,[36] based on a combination of DFT and experimental data. The force field has been slightly modified to accommodate version updates of MacroModel; the modified parameter subset used in the current work is available as Supporting Information. This force field, when utilized for structures similar to those in the training set, has a structural accuracy that rivals any other available method (including DFT),[36] and delivers conformational energies that from previous experience are accurate to within ca. 5−6 kJ/mol, slightly worse than the accuracy that can be obtained for small, purely organic molecules.[56] When further refined by B3LYP optimization, the conformational energy accuracy is usually improved to 1−2 kJ mol^{-1}, sufficient for a reliable comparison to experimental data. We want to identify all distinct conformations present in at least 5% (the approximate detection limit in the NMR experiments, vide supra), which translates to an energy range of ca. 8 kJ mol^{-1} above the global minimum at ambient temperature. Using a wide safety margin of 10 kJ mol^{-1}, this means that significantly different conformations within 18 kJ mol^{-1} from the global minimum in the MM conformational searches should be subjected to DFT validation.

Molecular modeling is basically a gas phase method, and for comparison with data determined in solvent, it is necessary to

(51) Hayashi, T.; Yamamoto, A.; Ito, Y.; Nishioka, E.; Miura, H.; Yanagi, K. *J. Am. Chem. Soc.* **1989**, *111*, 6301.
(52) For an example involving malononitriles in asymmetric decarboxylative cycloaddition of electron-deficient olefins see: (a) Wang, C.; Tunge, J. A. *J. Am. Chem. Soc.* **2008**, *130*, 8118.
(53) Berrisford, D. J.; Bolm, C.; Sharpless, K. B. *Angew. Chem., Int. Ed. Engl.* **1995**, *34*, 1059.
(54) (a) Norrby, P.-O.; Liljefors, T. *J. Comput. Chem.* **1998**, *19*, 1146. (b) Norrby, P.-O.; Brandt, P. *Coord. Chem. Rev.* **2001**, *212*, 79. (c) Norrby, P.-O. In *Computational Organometallic Chemistry*; Cundari, T. Ed.; Marcel Dekker: New York, 2001; pp 7−37.
(55) MM3* is a modification of the original MM3(89) force field: (a) Allinger, N. L.; Yuh, Y. H.; Lii, J.-H. *J. Am. Chem. Soc.* **1989**, *111*, 8551. (b) For some additions in the MM3(94) force field, see: Allinger, N. L.; Zhou, X.; Bergsma, J. *J. Mol. Struct. (Theochem)* **1994**, *312*, 69.

augment the modeling method by some type of solvent representation. For DFT and other quantum chemical techniques, reliable continuum methods are available (vide infra), but we know of no current solvation method that allows application to metal complexes in MM. The best method available to us was to simply screen electrostatic interactions by increasing the dielectric constant to 9, as a very rough simulation of dichloromethane or THF solvation, previously validated in similar applications.[57] Conformational searches employed the pseudo-systematic Monte Carlo Search[58] implemented in MacroModel,[59] with further fine-grained refinement using Low Mode Searching.[60]

All energies reported herein come from DFT optimization using the B3LYP functional[35] in conjunction with the LACVP* basis set.[61] Solvent effects were represented by the PBF continuum model[62] with default parameters for THF (solvent = tetrahydrofuran) and also CH_2Cl_2 (solvent = dichloromethane). As expected, the calculations in the two solvents gave virtually identical structures, and relative energies that agreed to within a few kJ mol^{-1}. All DFT structures and energies are available as Supporting Information. The B3LYP results agreed with the ordering of the MM conformations, even though individual relative energies were shifted by a few kJ mol^{-1}, in good agreement with previous usage of the force field.

We also studied reactions where **8**$^+$ was either the product or reactant, that is, ionization of cyclohexenyl acetate **5** by Pd(*R*,*R*-**1**) leading to **8**$^+$ and acetate anion, or nucleophilic attack of dimethyl malonate anion with or without alkali metal counterion on **8**$^+$ leading to **6** bound to Pd(*R*,*R*-**1**). Considerable previous experience has shown us that the combination of double-ζ basis set with a continuum solvation model is both necessary and sufficient for an accurate reproduction of (η^3-allyl)Pd reactivity.[37,43] In particular, it has been shown that in gas phase calculations, attack of a negative nucleophile on cationic (η^3-allyl)Pd complexes is a monotonous downhill process; there is no transition state.[37] Thus, continuum solvation is a requirement for location of the relevant stationary points. In the current project, as well as previously,[43] we have noted that the reaction coordinate has a long, flat region around the TS, sometimes with small bumps that are artifacts from the cavity model used for continuum solvation. In our experience, regular transition state searches frequently converge to a minor bump or flat region that may be quite far from the actual TS. On the other hand, the reaction coordinate is closely correlated with the C−Nu distance; a relaxed scan over this coordinate produces a relatively smooth curve without the sudden energy jumps ("snap effects") indicative of a discontinuity in the calculated reaction coordinate. The absence of discontinuities could also be verified by visual inspection and animation of the converged points along the path. Thus, choosing the highest point on a relaxed coordinate scan allows a reliable location of transition structures, validated by inspection of the PES. All "transition states" have been located this way. However, this procedure has a certain drawback. We are currently unable to calculate reliable frequencies for this size of complex in solvent. Therefore, we cannot calculate the vibrational contribution to the free energy, in particular the entropy component. Since higher energy, wider stationary points tend to also have higher entropies, we neglect a contribution that will tend to compensate some (but not all) of the calculated energy differences. Thus, we see that all large energy differences will be overestimated, sometimes severely. We are therefore careful to draw conclusions only from calculated trends, not absolute energy differences.

Acknowledgment. We thank AstraZeneca, EPSRC, University of Bristol, and the Federal Educational Department of the State of Aargau, Switzerland, for generous funding, Johnson Matthey for donation of $PdCl_2$, and Chirotech for donation of both enantiomers of the 'Standard Ligand' (**1**). The computations were performed on C3SE computing resources in Gothenburg. G.C.L.J. is a Royal Society Wolfson Research Merit Awardee, and P.O.N. is supported by the Swedish Research Council. Dr. H. Hagelin-Weaver (née Hagelin), Dr. I. J. S. Fairlamb, Dr. A. Martorell, Dr. P. M. Tomlin, and Mr. Antony Meadowcroft are thanked for preliminary studies.

Supporting Information Available: Details for preparation of Pd complexes **7**$^+$, **8**$^+$, d_9-**8**$^+$, and **8a**−**d**$^+$, together with NMR analyses and full computational details. This material is available free of charge via the Internet at http://pubs.acs.org.

JA8099757

(56) An error of ca 2 kJ mol^{-1} corresponds to a factor of 2 in the calculated populations at ambient temperature, for both equilibria and rates. Comparisons to experimental data for typical organic molecules indicate that this accuracy is achievable with well-parameterized molecular mechanics, and improved to slightly below 2 kJ mol^{-1} using B3LYP with a double-ζ basis set: (a) Liljefors, T.; Gundertofte, K.; Norrby, P.-O.; Pettersson, I. In *Computational Medicinal Chemistry for Drug Discovery*; Bultinck, P., Tollenaere, J. P., De Winter, H., Langenaeker, W., Eds.; Marcel Dekker: New York, 2004; p 1. (b) Gundertofte, K.; Liljefors, T.; Norrby, P.-O.; Pettersson, I. *J. Comput. Chem.* **1996**, *17*, 429. (c) Pettersson, I.; Liljefors, T. In *Reviews in Computational Chemistry*; Lipkowitz, K. B., Boyd, D. B., Eds.; VCH: New York, 1996; Vol. 9, p 167.

(57) Norrby, P.-O.; Åkermark, B.; Hæffner, F.; Hansson, S.; Blomberg, M. *J. Am. Chem. Soc.* **1993**, *115*, 4859.
(58) Goodman, J. M.; Still, W. C. *J. Comput. Chem.* **1991**, *12*, 1110.
(59) Maestro 8.5, MacroModel 9.5, and Jaguar 7.5, Schrodinger, LLC, New York, NY, 2008. For documentation and current versions of the programs see www.schrodinger.com.
(60) Kolossvary, I.; Guida, W. C. *J. Am. Chem. Soc.* **1996**, *118*, 5011.
(61) The LACVP* basis set uses 6-31G* for the lighter elements. Heavy metals (Pd, Cs, K) use the Hay−Wadt small-core ECP with accompanying basis set: Hay, P. J.; Wadt, W. R. *J. Chem. Phys.* **1985**, *82*, 299.
(62) (a) Tannor, D. J; Marten, B.; Murphy, R.; Friesner, R. A.; Sitkoff, D.; Nicholls, A.; Ringnalda, M.; Goddard, W. A., III; Honig, B. *J. Am. Chem. Soc.* **1994**, *116*, 11875. (b) Marten, B.; Kim, K.; Cortis, C.; Friesner, R. A.; Murphy, R. B.; Ringnalda, M. N.; Sitkoff, D.; Honig, B. *J. Phys. Chem.* **1996**, *100*, 11775.